Journal of
Mechanics of
Materials and Structures

msp

GEOMETRICAL NONLINEAR DYNAMIC ANALYSIS OF TENSEGRITY SYSTEMS VIA THE COROTATIONAL FORMULATION

Xiaodong Feng

An efficient finite element formulation is presented for geometrical nonlinear dynamic analysis of tensegrity systems based on the corotational formulation. In this method, large displacement of a space rod element is decomposed into a rigid body motion in the global coordinate system and a pure small deformation in the local coordinate system. A new form of tangent stiffness matrix, including both static and dynamic stages, is derived based on the proposed approach. The Newmark constant acceleration method in conjunction with modified Newton–Raphson method is employed to solve the nonlinear dynamic equation of motion. A five-module quadruplex tensegrity beam is given as the numerical example to illustrate the validity and efficiency of the proposed algorithm for geometrical nonlinear dynamic analysis of tensegrity structures.

1. Introduction

Research into active structures has been at the forefront of aerospace, biological, civil and mechanical engineering for recent years [Domer and Smith 2005; Ziegler 2005; Korkmaz 2011; Luo et al. 2008; Paul et al. 2006; Rovira and Tur 2009]. Advances in theory and practice of active structural control have changed the general perception of structures. Upon integration of active components, structures become dynamic objects capable of interacting with their environments. Increasingly, the ability to adapt to performance demands and environmental conditions has become key design criteria for a range of structural and mechanical systems. Among many structural topologies, the tensegrity might be the most promising actively controlled structures for its large motion amplitude and high strength-to-mass ratio [Adam and Smith 2008; Masic and Skelton 2006; Raja and Narayanan 2007; Sultan and Skelton 2003; Wroldsen et al. 2009; Skelton et al. 2014]. A fundamental aspect of tensegrities is the stress unilateral property of the compression: cables and struts must be under tension and compression, respectively. That is to say, the cables will be slacking when compressive loads are applied, which makes tensegrity systems flexible and easily controllable using small amounts of energy [Tibert and Pellegrino 2003; Juan and Tur 2008]. Another main requirement for a structure to be categorized as a tensegrity structure is that its initial pre-stressed configuration must be in stable equilibrium in absence of external forces, and which to a high degree decides the response properties, e.g. the stiffness to external loading. The design of a tensegrity structure thereby has to include these aspects in addition to the definition of a special geometry.

A complete analysis of the tensegrity structures comprises two parts. The first one is the evaluation of pre-stressed configurations, known as form-finding, which has been and is currently object of extensive research [Tibert and Pellegrino 2003]. The second part is the investigation of behavior under external

loads. In the literature, the form-finding step has been widely studied by different approaches [Barnes 1999; Xu and Luo 2010; Chen et al. 2012; Tran and Lee 2010; Koohestani and Guest 2013; Lee and Lee 2014; Feng and Guo 2015; Zhang et al. 2014]. On the other hand, however, the structure analysis step for nonlinear behavior, especially in the regime of large displacement, is still a difficult issue for structural engineers since tensegrities are in general both kinematically and statically indeterminate. Nevertheless, as is known to all, the total Lagrangian (TL) approach and update Lagrangian (UL) approach have been used widely for large-displacement analysis. Kebiche et al. [1999] performed a geometrical, nonlinear, elastic analysis for a basic quadruplex module (four-strut tensegrity prism) subjected to axial, flexural and torsional loads and a multi-cell beam under traction based on TL approach. Kebiche and Kahla [2000] developed nonlinear elasto-plastic investigations of a five quadruplex module tensegrity system based on an UL formulation. Murakami [2001] analyzed static and dynamic characteristics of tensegrity structure using both Eulerian and Lagrangian formulations of large-displacement kinematics and kinetics. The modal analysis performed by Murakmi indicated that the tensegrity had low natural frequency modes like thin members and it can be regarded as a typically flexible structure which usually has a complicated nonlinear behavior. Recently, Tran and Lee [2011] performed geometric and material analysis of tensegrity structures based on both total and updated Lagrangian formulations, and the updated Lagrangian formulation was recommended for large deflection analysis. Oliveto and Sivaselvan [2011] studied dynamic properties of tensegrity structures using a complementarity framework in the small displacement regime.

Lately, an alternative and more attractive approach, known as the corotational (CR) method, was proposed to investigate nonlinear behavior of tensegrity structures. Several researchers have proved that the CR formulation is computational more convenient and efficient for large-displacement and small-strain problems [Crisfield and Moita 1996; Felippa and Haugen 2005; Zhang et al. 2013; Zhang et al. 2015]. Relative literatures also demonstrated that the CR formulation offers exceptional benefits for an element which has more rigid body modes than deformational modes in a static analysis [Faroughi and Lee 2014; Feng and Guo 2017; Faroughi et al. 2017]. Because space rod element have five rigid body modes (three translations and two rotations) and only one deformational mode, i.e. the axial compression or extension, the CR formulation seems more attractive for the investigation of dynamic behavior of tensegrity systems. Although dynamic analysis of structural components (e.g. beam and membrane) have been performed successfully by the CR method [Le et al. 2011; Le et al. 2012; Eriksson and Faroughi 2013; Faroughi and Eriksson 2017], to our knowledge, dynamic analysis of tensegrity structures via the CR approach was rarely seen.

The main objective of this paper is to develop a 3D corotational model for geometrical nonlinear dynamic analysis of tensegrity structures. The CR formulation, which decomposes a large displacement into a rigid body motion and a pure small deformation, is adapted to achieve the internal force vector, the static tangent stiffness matrix, the inertial force vector, the mass matrix and the dynamic tangent stiffness matrix. By means of the CR approach, the space rod element is utilized to model the geometrical nonlinear dynamic behavior of tensegrity structures in local coordinates. The advantage of the proposed method is that behaviors of rod elements can be described utilizing engineering strain and stress which are calculated directly by the small-deformation elastic theory, although geometrical nonlinearity must be taken into account. The rod element has deformation only along its longitudinal direction (small strain), this makes the orientation of the 2nd and 3rd axes arbitrary and therefore torsion and bending

have been ignored in this paper. In the process of analyzing tensegrities at any equilibrium configuration with and without loads, the slackening constraints of cable elements have been taken into account. It is assumed that the form-finding procedure has been completed and the self-stress coefficients are known in advance [Feng and Guo 2015; Feng 2017].

The organization of this paper is as follows: Section 2 presents the derivations of the internal force vector, the static tangent stiffness matrix, the inertial force vector, the mass matrix and the dynamic tangent stiffness matrix. In Section 3, the Newmark constant acceleration method in conjunction with modified Newton–Raphson method are employed to solve the nonlinear dynamic equation of motion. A numerical example is performed to illustrate the validity and convergence of the proposed approach, which is presented in Section 4. Finally, some conclusions are summarized.

2. Global corotational formulation

In establishing the stress-strain relation to account for yielding behavior of an axially-loaded rod, the following assumptions are adopted for tensegrity structures:

- Members are connected by pin joints.
- Struts are elements that carry axial tensile or compressive forces.
- Cables are elements that carry only axial tensile forces.
- The materials are considered to be linear and elastic.
- The tensegrity structures are subjected to external load only at nodes.
- Both local and global buckling of strut element are not considered.
- There are no dissipative forces acting on the system.

2.1. *Derivation of the internal force vector.* Figure 1 displays a rod finite element with two end nodes (i, j). As can be seen, there are two coordinate systems. The first one is the global coordinate system XYZ and the other is the local coordinate system x_l, y_l, z_l that is fixed on and moves with the element. The initial configuration "ij" goes to the current configuration "$i''j'''$", via a large-rotation and small-strain motion. The motion can thus be divided into two steps. The first step is a rigid body motion and translation from the configuration "ij" to "$i'j'''$" in the global coordinate system XYZ; the second one is a small-strain deformation from the configuration "$i'j'''$" to "$i''j'''$" in the local coordinate system $x_l y_l z_l$. Therefore, the transformation relation between local and global coordinate systems needs to be found.

The element nodal coordinates at initial time and time t in the global coordinate system XYZ are denoted by $(^0x_i, {}^0y_i, {}^0z_i)$, $(^0x_j, {}^0y_j, {}^0z_j)$, $(^tx_i, {}^ty_i, {}^tz_i)$, $(^tx_j, {}^ty_j, {}^tz_j)$, respectively.

Thus, the global displacement vector is given by

$$\begin{aligned} \boldsymbol{d} &= \begin{bmatrix} u_i & v_i & w_i & u_j & v_j & w_j \end{bmatrix}^T \\ &= \begin{bmatrix} {}^tx_i - {}^0x_i & {}^ty_i - {}^0y_i & {}^tz_i - {}^0z_i & {}^tx_j - {}^0x_j & {}^ty_j - {}^0y_j & {}^tz_j - {}^0z_j \end{bmatrix}^T, \end{aligned} \tag{1}$$

and the local displacement along the rod element is
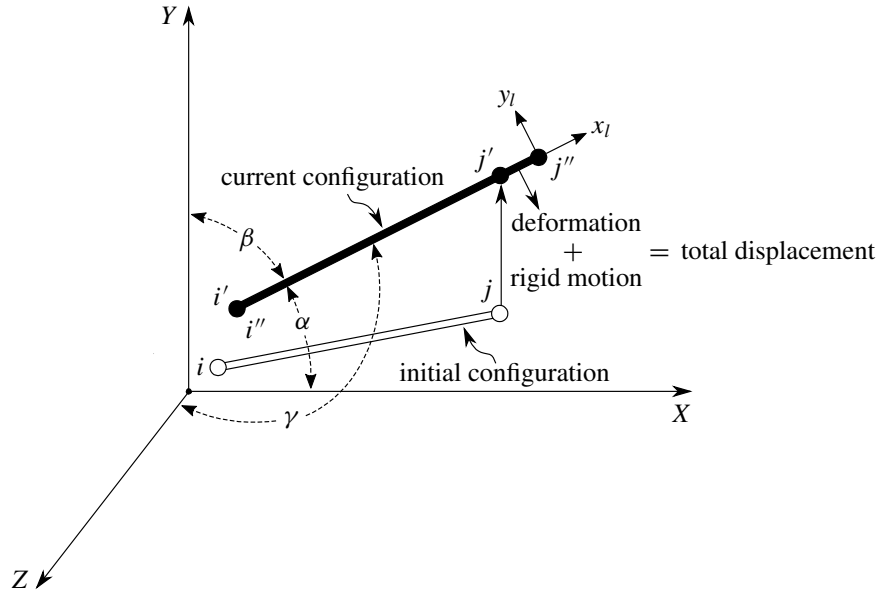
$$\Delta l = {}^tl - {}^0l, \tag{2}$$

Figure 1. Illustration of the corotational method of a space rod element.

where ^0l and ^tl are the lengths of the rod element at initial time and time t, respectively, given by

$$^0l = \sqrt{(^0x_j - {}^0x_i)^2 + (^0y_j - {}^0y_i)^2 + (^0z_j - {}^0z_i)^2}, \tag{3}$$

$$^tl = \sqrt{(^0x_j - {}^0x_i + u_j - u_i)^2 + (^0y_j - {}^0y_i + v_j - v_i)^2 + (^0z_j - {}^0z_i + w_j - w_i)^2}. \tag{4}$$

Let c_1, c_2 and c_3 be the cosine angles of the x_l-axis with respect to the global coordinate system XYZ:

$$c_1 = \cos\alpha = (^0x_j - {}^0x_i + u_j - u_i)/{}^tl$$
$$c_2 = \cos\beta = (^0y_j - {}^0y_i + v_j - v_i)/{}^tl \tag{5}$$
$$c_3 = \cos\gamma = (^0z_j - {}^0z_i + w_j - w_i)/{}^tl.$$

Taking the variation of (2) gives

$$\delta\Delta l = \delta{}^tl = \boldsymbol{t}\delta\boldsymbol{d}, \tag{6}$$

where

$$\boldsymbol{t} = \begin{bmatrix} -c_1 & -c_2 & -c_3 & c_1 & c_2 & c_3 \end{bmatrix}. \tag{7}$$

For cable elements, the local nodal internal force vector can be given by

$$q^l = \sigma A = E\varepsilon A, \tag{8}$$

where A is the cross-sectional area and σ is the stress of cables or struts. Engineering strain at time t can be calculated by

$$\varepsilon = \Delta l/{}^0l + \varepsilon_0, \tag{9}$$

in which ε_0 is the initial strain determined by pre-stressed or self-stress state.

Introducing (9) into (8), the local internal force vector can be rewritten as

$$q^l = \frac{EA}{^0l}\Delta l + EA\varepsilon_0. \tag{10}$$

Based on the principle of virtual work, i.e. the internal virtual work is equal in both the local and global coordinate systems, the relationship between the global nodal internal force vector $\boldsymbol{q}^g$ and local nodal internal force vector q^l is obtained from (12) as

$$\delta\boldsymbol{d}^T\boldsymbol{q}^g = (\delta\Delta l)^T q^l = (\boldsymbol{t}\delta\boldsymbol{d})^T \Rightarrow \boldsymbol{q}^g = \boldsymbol{t}^T q^l. \tag{11}$$

2.2. *Derivation of the static tangent stiffness matrix.* According to the static equilibrium relationship, the global tangent stiffness matrix $\overline{\boldsymbol{K}}_T$ is acquired from

$$\delta\boldsymbol{q}^g = \overline{\boldsymbol{K}}_T\delta\boldsymbol{d} = \overline{\boldsymbol{K}}_E\,\delta\boldsymbol{d} + \overline{\boldsymbol{K}}_G\,\delta\boldsymbol{d}, \tag{12}$$

where $\overline{\boldsymbol{K}}_E$ and $\overline{\boldsymbol{K}}_G$ denote the material and geometrical tangent stiffness matrices in the global coordinate system, respectively [Guest 2006].

Taking the variation of (11) gives

$$\delta\boldsymbol{q}^g = \boldsymbol{t}^T\delta q^l + \delta\boldsymbol{t}^T q^l. \tag{13}$$

Taking the variation of the local force vector q^l from (9), the first term in (13) can be obtained:

$$\delta q^l = \frac{EA}{^0l}\delta\Delta l = \frac{EA}{^0l}\boldsymbol{t}\delta\boldsymbol{d}. \tag{14}$$

In order to achieve the second term in (13), the variation of $\boldsymbol{t}$ from (7) is computed, results in

$$\delta\boldsymbol{t}^T = \frac{1}{^tl}\begin{bmatrix} 1-c_1^2 & -c_1c_2 & -c_1c_3 & c_1^2-1 & c_1c_2 & c_1c_3 \\ -c_1c_2 & 1-c_2^2 & -c_2c_3 & c_1c_2 & c_2^2-1 & c_2c_3 \\ -c_1c_3 & -c_2c_3 & 1-c_3^2 & c_1c_3 & c_2c_3 & c_3^2-1 \\ c_1^2-1 & c_1c_2 & c_1c_3 & 1-c_1^2 & -c_1c_2 & -c_1c_3 \\ c_1c_2 & c_2^2-1 & c_2c_3 & -c_1c_2 & 1-c_2^2 & -c_2c_3 \\ c_1c_3 & c_2c_3 & c_3^2-1 & -c_1c_3 & -c_2c_3 & 1-c_3^2 \end{bmatrix}\delta\boldsymbol{d} = \frac{1}{^tl}[\boldsymbol{R}\boldsymbol{R}^T - (\boldsymbol{R}\boldsymbol{r})(\boldsymbol{R}\boldsymbol{r})^T]\delta\boldsymbol{d}, \tag{15}$$

where matrix $\boldsymbol{R}$ and the vector $\boldsymbol{r}$ are as follows [Faroughi et al. 2015]:

$$\boldsymbol{R} = \begin{bmatrix} -1 & 0 & 0 & 1 & 0 & 0 \\ 0 & -1 & 0 & 0 & 1 & 0 \\ 0 & 0 & -1 & 0 & 0 & 1 \end{bmatrix}^T, \quad \boldsymbol{r} = \begin{Bmatrix} c_1 \\ c_2 \\ c_3 \end{Bmatrix}. \tag{16}$$

Introducing (10) into (13), the comparison between (14)–(15) and (12)–(13) gives the global tangent stiffness matrix as follows:

$$\overline{\boldsymbol{K}}_T = \frac{EA}{^0l}\boldsymbol{t}^T\boldsymbol{t} + \frac{\frac{EA}{^0l}\Delta l + EA\varepsilon_0}{^tl}[\boldsymbol{R}\boldsymbol{R}^T - (\boldsymbol{R}\boldsymbol{r})(\boldsymbol{R}\boldsymbol{r})^T]. \tag{17}$$
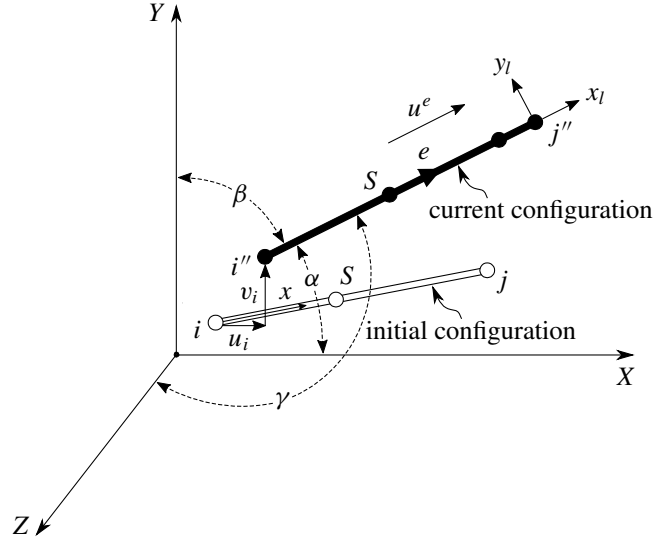
Figure 2. Illustration of the kinetic energy of a space rod element.

2.3. *Derivation of the inertial force vector and the mass matrix.* Using the notation shown in Figure 2, the global position can be written as

$$OS = (x_i + u_i)e_1 + (y_i + v_i)e_2 + (z_i + w_i)e_3 + \frac{{}^t l}{{}^0 l}(\cos\alpha \cdot e_1 + \cos\beta \cdot e_2 + \cos\gamma \cdot e_3), \qquad (18)$$

where e_1, e_2 and e_3 are the three unit coordinate vectors of the corresponding coordinate axes.

Therefore the global velocity components $\dot{u}$, $\dot{v}$ and $\dot{w}$ can be achieved from differentiating (18):

$$\dot{u} = \dot{u}_i + \frac{x}{{}^0 l}(\dot{u}_j - \dot{u}_i), \quad \dot{v} = \dot{v}_i + \frac{x}{{}^0 l}(\dot{v}_j - \dot{v}_i), \quad \dot{w} = \dot{w}_i + \frac{x}{{}^0 l}(\dot{w}_j - \dot{w}_i). \qquad (19)$$

The kinetic energy of a space rod element E (not to be confused with the same symbol used for the modulus of elasticity) can be obtained as

$$E = \frac{1}{2}\rho \int A\big((\dot{u})^2 + (\dot{v})^2 + (\dot{w})^2\big)\, dl, \qquad (20)$$

where ρ represents the density of the rod element.

Transforming (20) into the vector form, gives

$$E = \frac{1}{2}\dot{u}^T \overline{M}\dot{u}, \qquad (21)$$

where $\overline{M}$ is the global mass matrix of the rod element, which can be determined by

$$\overline{M} = T^T m^l\, T, \qquad (22)$$

where T and m^l are the rotational matrix and the local mass matrix of the rod element, given by

$$T = \begin{bmatrix} c_1 & c_2 & c_3 & 0 & 0 & 0 \\ 0 & 0 & 0 & c_1 & c_2 & c_3 \end{bmatrix}, \quad m^l = \frac{\rho A l}{6}\begin{bmatrix} 2 & 1 \\ 1 & 1 \end{bmatrix}.$$

The inertial force vector $\boldsymbol{q}^E$ can be computed from the (21) by employing the Lagrangian equation of motion, as

$$q^E = \frac{d}{dt}\left[\frac{\partial E}{\partial \dot{\boldsymbol{u}}}\right] - \left[\frac{\partial E}{\partial \boldsymbol{u}}\right]. \tag{23}$$

By substituting (21) into (23), the first term in (23) can be computed as

$$\frac{d}{dt}\left[\frac{\partial E}{\partial \dot{\boldsymbol{u}}}\right] = \overline{\boldsymbol{M}}\ddot{\boldsymbol{u}} + \dot{\overline{\boldsymbol{M}}}\dot{\boldsymbol{u}}. \tag{24}$$

Equation (22) indicates that the mass matrix $\overline{\boldsymbol{M}}$ is a function of c_1, c_2 and c_3, which are functions of time, thus

$$\dot{\overline{\boldsymbol{M}}} = \frac{\partial \overline{\boldsymbol{M}}}{\partial c_1}\dot{c}_1 + \frac{\partial \overline{\boldsymbol{M}}}{\partial c_2}\dot{c}_2 + \frac{\partial \overline{\boldsymbol{M}}}{\partial c_3}\dot{c}_3, \tag{25}$$

where c_1, c_2 and c_3 are calculated as

$$\dot{c}_1 = \frac{dc_1}{dt} = \frac{dc_1}{d\boldsymbol{u}}\frac{d\boldsymbol{u}}{dt} = \frac{\boldsymbol{t}_1^T}{{}^t l}\dot{\boldsymbol{u}}, \quad \dot{c}_2 = \frac{dc_2}{dt} = \frac{dc_2}{d\boldsymbol{u}}\frac{d\boldsymbol{u}}{dt} = \frac{\boldsymbol{t}_2^T}{{}^t l}\dot{\boldsymbol{u}}, \quad \dot{c}_3 = \frac{dc_3}{dt} = \frac{dc_3}{d\boldsymbol{u}}\frac{d\boldsymbol{u}}{dt} = \frac{\boldsymbol{t}_3^T}{{}^t l}\dot{\boldsymbol{u}}, \tag{26}$$

and

$$\begin{aligned}
\boldsymbol{t}_1 &= \begin{bmatrix} c_1^2 - 1 & c_1 c_2 & c_1 c_3 & 1 - c_1^2 & -c_1 c_2 & -c_1 c_3 \end{bmatrix}^T, \\
\boldsymbol{t}_2 &= \begin{bmatrix} c_1 c_2 & c_2^1 - 1 & c_2 c_3 & -c_1 c_2 & 1 - c_2^2 & -c_2 c_3 \end{bmatrix}^T, \\
\boldsymbol{t}_3 &= \begin{bmatrix} c_1 c_3 & c_2 c_3 & c_3^2 - 1 & -c_1 c_3 & -c_2 c_3 & 1 - c_3^2 \end{bmatrix}^T.
\end{aligned} \tag{27}$$

The partial derivates in (25) are calculated as

$$\begin{aligned}
\frac{\partial \overline{\boldsymbol{M}}}{\partial c_1} &= \overline{\boldsymbol{M}}_{c_1} = \frac{\partial \boldsymbol{T}^T}{\partial c_1}\boldsymbol{m}^l \boldsymbol{T} + \boldsymbol{T}^T \boldsymbol{m}^l \frac{\partial \boldsymbol{T}}{\partial c_1} = \boldsymbol{R}_1^T \boldsymbol{m}^l \boldsymbol{T} + \boldsymbol{T}^T \boldsymbol{m}^l \boldsymbol{R}_1, \\
\frac{\partial \overline{\boldsymbol{M}}}{\partial c_2} &= \overline{\boldsymbol{M}}_{c_2} = \frac{\partial \boldsymbol{T}^T}{\partial c_2}\boldsymbol{m}^l \boldsymbol{T} + \boldsymbol{T}^T \boldsymbol{m}^l \frac{\partial \boldsymbol{T}}{\partial c_2} = \boldsymbol{R}_2^T \boldsymbol{m}^l \boldsymbol{T} + \boldsymbol{T}^T \boldsymbol{m}^l \boldsymbol{R}_2, \\
\frac{\partial \overline{\boldsymbol{M}}}{\partial c_3} &= \overline{\boldsymbol{M}}_{c_3} = \frac{\partial \boldsymbol{T}^T}{\partial c_3}\boldsymbol{m}^l \boldsymbol{T} + \boldsymbol{T}^T \boldsymbol{m}^l \frac{\partial \boldsymbol{T}}{\partial c_3} = \boldsymbol{R}_3^T \boldsymbol{m}^l \boldsymbol{T} + \boldsymbol{T}^T \boldsymbol{m}^l \boldsymbol{R}_3,
\end{aligned} \tag{28}$$

where

$$\begin{aligned}
\boldsymbol{R}_1 &= \frac{\partial \boldsymbol{T}}{\partial c_1} = \begin{bmatrix} 1 & -c_1/c_2 & -c_1/c_3 & 0 & 0 & 0 \\ 0 & 0 & 0 & 1 & -c_1/c_2 & -c_1/c_3 \end{bmatrix}, \\
\boldsymbol{R}_2 &= \frac{\partial \boldsymbol{T}}{\partial c_2} = \begin{bmatrix} -c_2/c_1 & 1 & -c_2/c_3 & 0 & 0 & 0 \\ 0 & 0 & 0 & -c_2/c_1 & 1 & -c_2/c_3 \end{bmatrix}, \\
\boldsymbol{R}_3 &= \frac{\partial \boldsymbol{T}}{\partial c_3} = \begin{bmatrix} -c_3/c_1 & -c_3/c_2 & 1 & 0 & 0 & 0 \\ 0 & 0 & 0 & -c_3/c_1 & -c_3/c_2 & 1 \end{bmatrix}.
\end{aligned} \tag{29}$$

By substituting (21) into (23), the second term in (23) can be computed as

$$\begin{aligned}
\left[\frac{\partial E}{\partial \boldsymbol{u}}\right] &= \frac{\partial E}{\partial c_1}\frac{\partial c_1}{\partial \boldsymbol{u}} + \frac{\partial E}{\partial c_2}\frac{\partial c_2}{\partial \boldsymbol{u}} + \frac{\partial E}{\partial c_3}\frac{\partial c_3}{\partial \boldsymbol{u}} \\
&= \left(\frac{1}{2}\dot{\boldsymbol{u}}^T \frac{\partial \overline{\boldsymbol{M}}}{\partial c_1}\dot{\boldsymbol{u}}\right)\frac{\boldsymbol{t}_1}{{}^t l} + \left(\frac{1}{2}\dot{\boldsymbol{u}}^T \frac{\partial \overline{\boldsymbol{M}}}{\partial c_2}\dot{\boldsymbol{u}}\right)\frac{\boldsymbol{t}_2}{{}^t l} + \left(\frac{1}{2}\dot{\boldsymbol{u}}^T \frac{\partial \overline{\boldsymbol{M}}}{\partial c_3}\dot{\boldsymbol{u}}\right)\frac{\boldsymbol{t}_3}{{}^t l}.
\end{aligned} \tag{30}$$

Hence, the expression of the inertial force vector can be obtained by substituting (24) and (30) into (23):

$$q^E = \overline{M}\ddot{u} + \dot{\overline{M}}\dot{u} - \left(\frac{1}{2}\dot{u}^T \frac{\partial \overline{M}}{\partial c_1}\dot{u}\right)\frac{t_1}{{}^t l} - \left(\frac{1}{2}\dot{u}^T \frac{\partial \overline{M}}{\partial c_2}\dot{u}\right)\frac{t_2}{{}^t l} - \left(\frac{1}{2}\dot{u}^T \frac{\partial \overline{M}}{\partial c_3}\dot{u}\right)\frac{t_3}{{}^t l}. \tag{31}$$

2.4. Derivation of the dynamic tangent stiffness matrix. The dynamic tangent stiffness matrix $\overline{K}_{D,t}$ can be written as

$$\overline{K}_{D,t} = \frac{\partial q^g}{\partial u}\Big|_t + \frac{\partial q^E}{\partial u}\Big|_t. \tag{32}$$

Differentiating the global nodal internal force vector q^g and the inertial force vector q^E with respect to displacement, velocity and acceleration, the static tangent stiffness matrix, mass matrix and gyroscopic matrix are given as

$$\overline{K}_T = \frac{\partial q^g}{\partial u}, \quad \overline{M} = \frac{\partial q^E}{\partial \ddot{u}}, \quad \overline{C} = \frac{\partial q^E}{\partial \dot{u}} = \dot{\overline{M}} + \overline{H} - \overline{H}^T, \tag{33}$$

where

$$\overline{H} = \frac{\partial M}{\partial c_1}\left(\dot{u}\frac{t_1^T}{{}^t l}\right) + \frac{\partial M}{\partial c_2}\left(\dot{u}\frac{t_2^T}{{}^t l}\right) + \frac{\partial M}{\partial c_3}\left(\dot{u}\frac{t_3^T}{{}^t l}\right). \tag{34}$$

To get $\partial q^E/\partial u$, the derivative of each term of (31) with respect to the displacement is calculated as

$$\overline{K}_{E,1} = \frac{\partial \overline{M}\ddot{u}}{\partial u} = \frac{\partial \overline{M}}{\partial c_1}\left(\ddot{u}\frac{t_1^T}{{}^t l}\right) + \frac{\partial \overline{M}}{\partial c_2}\left(\ddot{u}\frac{t_2^T}{{}^t l}\right) + \frac{\partial \overline{M}}{\partial c_3}\left(\ddot{u}\frac{t_3^T}{{}^t l}\right) = \overline{M}_{c_1}\ddot{u}\frac{t_1^T}{{}^t l} + \overline{M}_{c_2}\ddot{u}\frac{t_2^T}{{}^t l} + \overline{M}_{c_3}\ddot{u}\frac{t_3^T}{{}^t l}, \tag{35}$$

$$\begin{aligned}
\overline{K}_{E,2} = \frac{\partial \dot{\overline{M}}\dot{u}}{\partial u} &= \left(\frac{t_1^T}{{}^t l}\dot{u}\right)\left(\frac{\partial \overline{M}_{c_1}}{\partial c_1}\left(\dot{u}\frac{t_1^T}{{}^t l}\right) + \frac{\partial \overline{M}_{c_1}}{\partial c_2}\left(\dot{u}\frac{t_2^T}{{}^t l}\right) + \frac{\partial \overline{M}_{c_1}}{\partial c_3}\left(\dot{u}\frac{t_3^T}{{}^t l}\right)\right) \\
&\quad + \left(\frac{t_2^T}{{}^t l}\dot{u}\right)\left(\frac{\partial \overline{M}_{c_2}}{\partial c_1}\left(\dot{u}\frac{t_1^T}{{}^t l}\right) + \frac{\partial \overline{M}_{c_2}}{\partial c_2}\left(\dot{u}\frac{t_2^T}{{}^t l}\right) + \frac{\partial \overline{M}_{c_2}}{\partial c_3}\left(\dot{u}\frac{t_3^T}{{}^t l}\right)\right) \\
&\quad + \left(\frac{t_3^T}{{}^t l}\dot{u}\right)\left(\frac{\partial \overline{M}_{c_3}}{\partial c_1}\left(\dot{u}\frac{t_1^T}{{}^t l}\right) + \frac{\partial \overline{M}_{c_3}}{\partial c_2}\left(\dot{u}\frac{t_2^T}{{}^t l}\right) + \frac{\partial \overline{M}_{c_3}}{\partial c_3}\left(\dot{u}\frac{t_3^T}{{}^t l}\right)\right) \\
&\quad + \overline{M}_{c_1}\dot{u}\dot{u}^T \frac{\partial(t_1^T/{}^t l)}{\partial u} + \overline{M}_{c_2}\dot{u}\dot{u}^T \frac{\partial(t_2^T/{}^t l)}{\partial u} + \overline{M}_{c_3}\dot{u}\dot{u}^T \frac{\partial(t_3^T/{}^t l)}{\partial u},
\end{aligned} \tag{36}$$

$$\begin{aligned}
\overline{K}_{E,3} = &\left(\dot{u}^T \frac{\partial \overline{M}_{c_1}}{\partial c_1}\dot{u}\right)\frac{t_1 t_1^T}{{}^t l^2} + \left(\dot{u}^T \frac{\partial \overline{M}_{c_1}}{\partial c_2}\dot{u}\right)\frac{t_1 t_2^T}{{}^t l^2} + \left(\dot{u}^T \frac{\partial \overline{M}_{c_1}}{\partial c_3}\dot{u}\right)\frac{t_1 t_3^T}{{}^t l^2} \\
&+ \left(\dot{u}^T \frac{\partial \overline{M}_{c_2}}{\partial c_1}\dot{u}\right)\frac{t_2 t_1^T}{{}^t l^2} + \left(\dot{u}^T \frac{\partial \overline{M}_{c_2}}{\partial c_2}\dot{u}\right)\frac{t_2 t_2^T}{{}^t l^2} + \left(\dot{u}^T \frac{\partial \overline{M}_{c_3}}{\partial c_3}\dot{u}\right)\frac{t_2 t_3^T}{{}^t l^2} \\
&+ \left(\dot{u}^T \frac{\partial \overline{M}_{c_3}}{\partial c_1}\dot{u}\right)\frac{t_3 t_1^T}{{}^t l^2} + \left(\dot{u}^T \frac{\partial \overline{M}_{c_3}}{\partial c_2}\dot{u}\right)\frac{t_3 t_2^T}{{}^t l^2} + \left(\dot{u}^T \frac{\partial \overline{M}_{c_3}}{\partial c_3}\dot{u}\right)\frac{t_3 t_3^T}{{}^t l^2} \\
&+ \left(\dot{u}^T \frac{\partial \overline{M}_{c_1}}{\partial c_1}\dot{u}\right)\frac{\partial(t_1^T/{}^t l)}{\partial u} + \left(\dot{u}^T \frac{\partial \overline{M}_{c_2}}{\partial c_1}\dot{u}\right)\frac{\partial(t_2^T/{}^t l)}{\partial u} + \left(\dot{u}^T \frac{\partial \overline{M}_{c_3}}{\partial c_1}\dot{u}\right)\frac{\partial(t_3^T/{}^t l)}{\partial u}. \tag{37}
\end{aligned}$$

The second derivatives of the mass matrix with respect to c_1, c_2 and c_3 in (35)–(37) are

$$\frac{\partial \overline{\boldsymbol{M}}_{c_1}}{\partial c_j} = \frac{\partial \boldsymbol{R}_i^T}{\partial c_j} \boldsymbol{m}^l \boldsymbol{T} + \boldsymbol{R}_i^T \boldsymbol{m}^l \frac{\partial \boldsymbol{T}}{\partial c_j} + \frac{\partial \boldsymbol{T}^T}{\partial c_j} \boldsymbol{m}^l \boldsymbol{R}_i + \boldsymbol{T}^T \boldsymbol{m}^l \frac{\partial \boldsymbol{R}_i}{\partial c_j} \quad \text{for} \quad i, j = 1, 2, 3 \tag{38}$$

and

$$\frac{\partial (\boldsymbol{t}_1^T / {}^t l)}{\partial \boldsymbol{u}} = \frac{(\partial \boldsymbol{t}_i / \partial \boldsymbol{u})\,{}^t l - \boldsymbol{t}_i (\partial\, {}^t l / \partial \boldsymbol{u})}{{}^t l^2} = \frac{(\partial \boldsymbol{t}_i / \partial \boldsymbol{u})\,{}^t l - \boldsymbol{t}_i \boldsymbol{t}}{{}^t l^2} \quad \text{for} \quad i, j = 1, 2, 3, \tag{39}$$

where $\boldsymbol{t}_i$ and $\boldsymbol{t}$ are determined by (27) and (7). Taking into account that $c_1^2 + c_2^2 + c_3^2 = 1$ and that each $\partial \boldsymbol{t}_i / \partial \boldsymbol{u}$ ($i = 1, 2, 3$) is a 6×6 matrix, the partials $\partial \boldsymbol{R}_i / \partial c_j$ and $\partial \boldsymbol{t}_i / \partial \boldsymbol{u}$ can be given as

$$\frac{\partial \boldsymbol{R}_1}{\partial c_1} = \begin{bmatrix} 0 & (c_3^2-1)/c_2^3 & (c_2^2-1)/c_3^3 & 0 & 0 & 0 \\ 0 & 0 & 0 & 0 & (c_3^2-1)/c_2^3 & (c_2^2-1)/c_3^3 \end{bmatrix}, \tag{40}$$

$$\frac{\partial \boldsymbol{R}_2}{\partial c_1} = \begin{bmatrix} (c_3^2-1)/c_1^3 & 0 & (c_2^2-1)/c_3^3 & 0 & 0 & 0 \\ 0 & 0 & 0 & (1-c_3^2)/c_1 c_2^2 & 0 & c_1(c_3^2-c_2^2)/c_2 c_3 \end{bmatrix}, \tag{41}$$

$$\frac{\partial \boldsymbol{R}_3}{\partial c_1} = \begin{bmatrix} (1-c_2^2)/c_3 c_1^2 & c_1(c_2^2-c_3^2)/c_3 c_2^3 & 0 & 0 & 0 & 0 \\ 0 & 0 & 0 & (1-c_2^2)/c_3 c_1^2 & c_1(c_2^2-c_3^2)/c_3 c_2^3 & 0 \end{bmatrix}, \tag{42}$$

$$\frac{\partial \boldsymbol{R}_2}{\partial c_2} = \begin{bmatrix} (c_3^2-1)/c_2^3 & 0 & (c_2^2-1)/c_3^3 & 0 & 0 & 0 \\ 0 & 0 & 0 & (c_3^2-1)/c_2^3 & 0 & (c_2^2-1)/c_3^3 \end{bmatrix}, \tag{43}$$

$$\frac{\partial \boldsymbol{R}_1}{\partial c_2} = \begin{bmatrix} 0 & (1-c_3^2)/c_1 c_2^2 & c_2(c_3^2-c_1^2)/c_1 c_3^3 & 0 & 0 & 0 \\ 0 & 0 & 0 & 0 & (1-c_3^2)/c_1 c_2^2 & c_2(c_3^2-c_1^2)/c_1 c_3^3 \end{bmatrix}, \tag{44}$$

$$\frac{\partial \boldsymbol{R}_3}{\partial c_2} = \begin{bmatrix} c_2(c_1^2-c_3^2)/c_1 c_3^3 & (1-c_1^2)/c_3 c_2^3 & 0 & 0 & 0 & 0 \\ 0 & 0 & 0 & c_2(c_1^2-c_3^2)/c_1 c_3^3 & (1-c_1^2)/c_3 c_2^3 & 0 \end{bmatrix}, \tag{45}$$

$$\frac{\partial \boldsymbol{R}_3}{\partial c_3} = \begin{bmatrix} (c_2^2-1)/c_1^3 & (c_1^2-1)/c_2^3 & 0 & 0 & 0 & 0 \\ 0 & 0 & 0 & (c_2^2-1)/c_1^3 & (c_1^2-1)/c_2^3 & 0 \end{bmatrix}, \tag{46}$$

$$\frac{\partial \boldsymbol{R}_1}{\partial c_3} = \begin{bmatrix} 0 & c_3(c_2^2-c_1^2)/c_1 c_2^3 & (1-c_2^2)/c_1 c_3^2 & 0 & 0 & 0 \\ 0 & 0 & 0 & 0 & c_3(c_2^2-c_1^2)/c_1 c_2^3 & (1-c_2^2)/c_1 c_3^2 \end{bmatrix}, \tag{47}$$

$$\frac{\partial \boldsymbol{R}_2}{\partial c_3} = \begin{bmatrix} c_3(c_1^2-c_2^2)/c_1 c_2^3 & 0 & (1-c_1^2)/c_2 c_3^2 & 0 & 0 & 0 \\ 0 & 0 & 0 & c_3(c_1^2-c_2^2)/c_1 c_2^3 & 0 & (1-c_1^2)/c_2 c_3^2 \end{bmatrix}, \tag{48}$$

$$\frac{\partial \boldsymbol{t}_1}{\partial \boldsymbol{u}} = \left[2c_1 \frac{\boldsymbol{t}_1^T}{{}^t l} \quad c_2 \frac{\boldsymbol{t}_1^T}{{}^t l} + c_1 \frac{\boldsymbol{t}_2^T}{{}^t l} \quad c_3 \frac{\boldsymbol{t}_1^T}{{}^t l} + c_1 \frac{\boldsymbol{t}_3^T}{{}^t l} \quad -2c_1 \frac{\boldsymbol{t}_1^T}{{}^t l} \quad -\left(c_2 \frac{\boldsymbol{t}_1^T}{{}^t l} + c_1 \frac{\boldsymbol{t}_2^T}{{}^t l}\right) \quad -\left(c_3 \frac{\boldsymbol{t}_1^T}{{}^t l} + c_1 \frac{\boldsymbol{t}_3^T}{{}^t l}\right) \right]^T, \tag{49}$$

$$\frac{\partial \boldsymbol{t}_2}{\partial \boldsymbol{u}} = \left[c_2 \frac{\boldsymbol{t}_1^T}{{}^t l} + c_1 \frac{\boldsymbol{t}_2^T}{{}^t l} \quad 2c_2 \frac{\boldsymbol{t}_2^T}{{}^t l} \quad c_3 \frac{\boldsymbol{t}_2^T}{{}^t l} + c_2 \frac{\boldsymbol{t}_3^T}{{}^t l} \quad -\left(c_2 \frac{\boldsymbol{t}_1^T}{{}^t l} + c_1 \frac{\boldsymbol{t}_2^T}{{}^t l}\right) \quad -2c_2 \frac{\boldsymbol{t}_2^T}{{}^t l} \quad -\left(c_3 \frac{\boldsymbol{t}_2^T}{{}^t l} + c_2 \frac{\boldsymbol{t}_3^T}{{}^t l}\right) \right]^T, \tag{50}$$

$$\frac{\partial \boldsymbol{t}_3}{\partial \boldsymbol{u}} = \left[c_3 \frac{\boldsymbol{t}_1^T}{{}^t l} + c_1 \frac{\boldsymbol{t}_3^T}{{}^t l} \quad c_3 \frac{\boldsymbol{t}_2^T}{{}^t l} + c_2 \frac{\boldsymbol{t}_3^T}{{}^t l} \quad 2c_3 \frac{\boldsymbol{t}_3^T}{{}^t l} \quad -\left(c_3 \frac{\boldsymbol{t}_1^T}{{}^t l} + c_1 \frac{\boldsymbol{t}_3^T}{{}^t l}\right) \quad -\left(c_3 \frac{\boldsymbol{t}_2^T}{{}^t l} + c_2 \frac{\boldsymbol{t}_3^T}{{}^t l}\right) \quad -2c_3 \frac{\boldsymbol{t}_3^T}{{}^t l} \right]^T. \tag{51}$$

Hence, the expression of $\partial \boldsymbol{q}^E / \partial \boldsymbol{u}$ is achieved by integrating (31) and (35)–(37):

$$\frac{\partial \boldsymbol{q}^E}{\partial \boldsymbol{u}} = \overline{\boldsymbol{K}}_E = \overline{\boldsymbol{K}}_{E,1} + \overline{\boldsymbol{K}}_{E,2} + \overline{\boldsymbol{K}}_{E,3} \,. \tag{52}$$

Substituting (17), (33) and (35)–(37) into (32), the dynamic tangent stiffness matrix can be obtained as

$$\overline{\boldsymbol{K}}_D = \overline{\boldsymbol{K}}_T + \overline{\boldsymbol{K}}_E + \frac{4}{\Delta t^2}\overline{\boldsymbol{M}} + \frac{2}{\Delta t}\overline{\boldsymbol{C}}, \tag{53}$$

where Δt denotes the time step.

Once the aforementioned vectors and matrices are acquired, the classical finite element method is utilized to assemble the global structural dynamic tangent stiffness matrix and mass matrix as

$$\overline{\boldsymbol{K}}_D = \sum \boldsymbol{L}\overline{\boldsymbol{K}}_D \boldsymbol{L}^T, \tag{54}$$

$$\boldsymbol{M} = \sum \boldsymbol{L}\overline{\boldsymbol{M}} \boldsymbol{L}^T, \tag{55}$$

where $\boldsymbol{L}$ is the element connectivity matrix, derived from structural topology and sums extend over all elements.

3. Nonlinear analysis process

The equation of dynamic equilibrium of tensegrity structures can be written as follows:

$$\boldsymbol{q}^E(\boldsymbol{u}, \dot{\boldsymbol{u}}, \ddot{\boldsymbol{u}}) = \boldsymbol{q}^{\text{ext}} - \boldsymbol{q}^g(\boldsymbol{u}), \tag{56}$$

where $\boldsymbol{q}^E$, $\boldsymbol{q}^{\text{ext}}$ and $\boldsymbol{q}^g$ represent the inertial, external and internal force vectors respectively. Note that if the seismic case is simulated, the external force $\boldsymbol{q}^{\text{ext}}$ should be replaced by $\boldsymbol{q}^{\text{ext}} - \boldsymbol{M}\ddot{\boldsymbol{u}}_g$, where $\ddot{\boldsymbol{u}}_g$ is the accelerationc vector of ground motion.

Discretization of (56) at time t gives

$$\boldsymbol{q}_{i,t} = \boldsymbol{q}_t^E(\boldsymbol{u}, \dot{\boldsymbol{u}}, \ddot{\boldsymbol{u}}) + \boldsymbol{q}_t^g(\boldsymbol{u}). \tag{57}$$

Hence

$$\boldsymbol{h}_t = \boldsymbol{q}_{i,t} - \boldsymbol{q}_t^{\text{ext}} = \boldsymbol{0}, \tag{58}$$

where $\boldsymbol{h}_t$ is the equivalent dynamic out of balance forces.

Introducing the predictor-corrector method [Kim and Yong 2001], equation (56) can be solved by using a Taylor series; thus the term $\boldsymbol{q}_{i,t+\Delta t}$ can be written as

$$\boldsymbol{q}_{i,t+\Delta t} = \boldsymbol{q}_{i,t} \left.\frac{\partial \boldsymbol{q}_{i,t+\Delta t}}{\partial \boldsymbol{u}}\right|_t (\boldsymbol{u}_{t+\Delta t} - \boldsymbol{u}_t) = \boldsymbol{q}_{i,t} + \boldsymbol{K}_{D,t}\Delta \boldsymbol{u}. \tag{59}$$

Substituting (59) into (57), the expected incremental predictor step can be computed as

$$\Delta \boldsymbol{u} = \boldsymbol{K}_{D,t}^{-1}(\boldsymbol{q}_{t+\Delta t}^{\text{ext}} - \boldsymbol{q}_t^{\text{ext}}). \tag{60}$$

By using the Newmark-average acceleration method, the updated displacement, velocity and acceleration are calculated:

$$u_{t+\Delta t} = u_t + \Delta u, \tag{61}$$

$$\dot{u}_{t+\Delta t} = \dot{u}_t + \Delta u \left(\frac{3}{4} \ddot{u}_t + \left(\frac{1}{2\Delta t^2} (u_{t+\Delta t} - u_t) - \frac{1}{2\Delta t} \dot{u}_t \right) \right), \tag{62}$$

$$\ddot{u}_{t+\Delta t} = \frac{2}{\Delta t^2} (u_{t+\Delta t} - u_t) - \frac{2}{\Delta t} \dot{u}_t. \tag{63}$$

In order that the equivalent dynamic out of balance forces can be approached to zero at each time step, the updated Newton–Raphson method should be utilized. Therefore, the improvement terms can be calculated as

$$\delta u_{t+\Delta t} = -K_{D,t+\Delta t}^{-1} h_{t+\Delta t}, \tag{64}$$

$$\delta \dot{u}_{t+\Delta t} = \frac{1}{2\Delta t} \delta u_{t+\Delta t}, \tag{65}$$

$$\delta \ddot{u}_{t+\Delta t} = \frac{2}{\Delta t^2} \delta u_{t+\Delta t}. \tag{66}$$

This procedure is then repeated until the value of nodal displacements and the equivalent dynamic out of balance forces fall below the threshold given as

$$\kappa = \max \left(\frac{\|\Delta u\|_2}{\|u_{t+\Delta t}\|_2}, \frac{\|q^{\text{ext}} - q^g\|_2}{\|q^{\text{ext}}\|_2} \right) < \text{Tol} = 10^{-6}. \tag{67}$$

Since slackening is a natural property of cables, the slackening of cable elements is taken into account in the following manner: the actual length of each cable is calculated and compared to its rest length within each iteration. If the rest length is longer than the actual length, the cable is assumed to be slack. Accordingly, its stiffness is not considered in the global structural system, and its axial force is set to zero.

4. Illustrative example

A five-module tensegrity beam (Figure 3; modules numbered M1 to M5) analyzed in [Kahla and Kebiche 2000] and [Tran and Lee 2011] is used to illustrate the proposed method. Eight infinitesimal mechanisms and nine independent self-stress modes are determined based on the rank deficiency equilibrium matrix for the tensegrity beam. In order to eliminate all the infinitesimal mechanisms, this tensegrity beam should be in the feasible self-stress mode which is a linear combination of the above nine independent self-stress modes [Tran and Lee 2010]. The initial self-stress coefficients of the structure can be determined by the mature form-finding methods [Tibert and Pellegrino 2003; Feng and Guo 2015]. Table 1 gives the initial self-stress values and material properties of the five-module quadruplex tensegrity beam.

Before observing the dynamic properties of the tensegrity beam under different seismic excitations, the modal analysis is performed as to give an intuitionistic knowledge of the natural vibration characteristics of this structure. Table 2 gives the first eight natural frequencies of the tensegrity beam modal. It is apparent that the structural natural frequencies are gradually increasing. Isometric views of the first
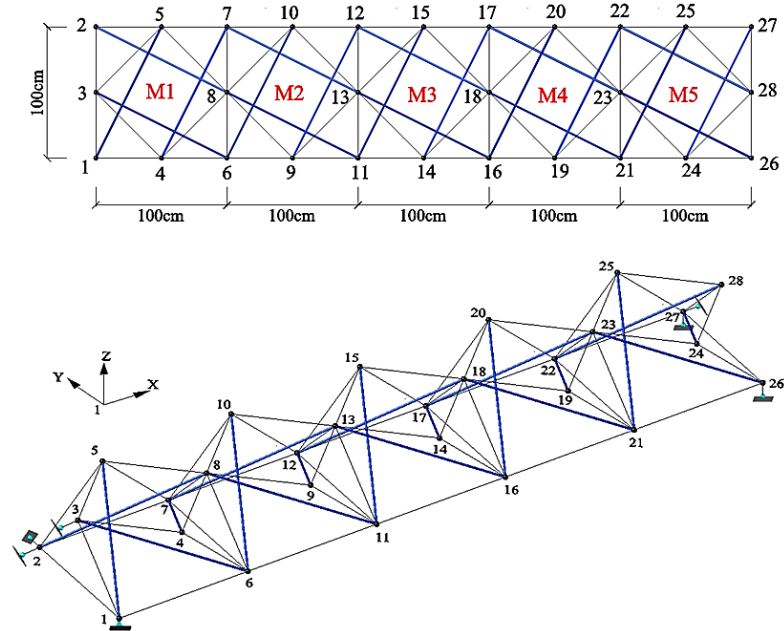
Figure 3. Geometry of a five-module quadruplex tensegrity beam: top view and perspective view.

Element	Category	Stress/KN for module #					Cross section/cm^2	Modulus /GPa
		1	2	3	4	5		
1		3.889	3.753	3.723	3.679	3.719		
2	Lower	6.870	6.517	6.552	6.559	6.963		
3	cables	3.700	7.253	6.875	6.913	6.913	0.280	40
4		7.253	6.875	6.913	6.913	3.705		
5		5.173	4.639	4.681	6.875	5.180		
6	Upper	5.158	5.040	5.053	5.040	5.180		
7	cables	5.129	4.639	4.681	4.639	5.180	0.280	40
8		5.250	5.084	5.095	5.084	5.180		
9		5.262	5.084	5.095	5.084	5.180		
10	Bracing	4.950	4.459	4.488	4.671	5.180		
11	cables	5.158	4.639	4.681	4.639	5.180	0.280	40
12		5.233	5.158	5.312	5.296	5.477		
13		−9.063	−8.472	−8.514	−8.472	−9.041		
14	Struts	−9.063	−8.472	−8.514	−8.472	−8.971		
15		−9.063	−8.780	−8.776	−8.780	−8.971	3.250	200
16		−8.934	−8.034	−8.108	−8.034	−8.971		

Table 1. Initial self-stress values and material properties of the five-module quadruplex tensegrity beam.

Mode	1	2	3	4	5	6	7	8	9	10
Frequency (Hz)	2.7	5.8	12.0	14.8	18.1	21.1	28.9	36.5	45.9	62.5

Table 2. Natural frequencies of the quadruplex unit modal (first eight modes).

four mode shapes are displayed in Figure 4, indicating that the lower order mode shapes are almost symmetrical or anti-symmetrical, while the higher order modes that involve synchronous and asynchronous deformation of adjacent modules can not be identified clearly. This might be explained by the asymmetry of the structure, i.e. the basic module and the placements of the boundary supports are not perfectly symmetrical.
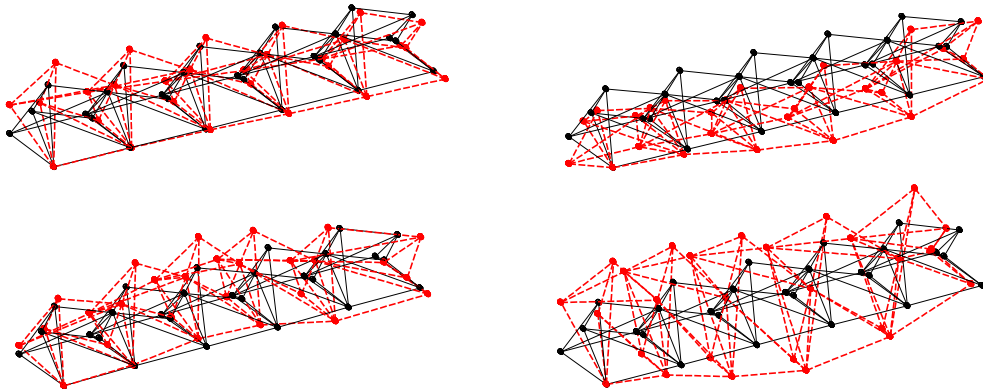
Figure 4. Mode shapes of the first four natural frequencies. Top: Mode 1 (twisting) and Mode 2 (bending). Bottom: Mode 3 (bending) and Mode 4 (higher-order).

To compare the dynamic responses of the tensegrity beam under different seismic excitations, the El Centro and the Taft earthquake data (Figure 5) is employed. The sampling time and time step size are taken as 20 s and 0.02 s, respectively. Figure 6 plots the time history response curves of typical nodal displacements of the tensegrity beam under El Centro seismic wave and Taft seismic wave. Table 3 gives the comparison of the maximum displacements of the specified nodes excited by these two different seismic waves. The numerical results from Figure 6 and Table 3 indicate that the maximum nodal displacements are less differentiating at some level considering two seismic waves, i.e. the nodal displacement distributions are approximately the same. Additionally, the possible maximum structural deflections (node 15) are 0.0209 m (El Centro) and 0.0217 m (Taft) which are less than 1/200 of the beam span. It indicates that the structure will not be damaged due to excessive deformation, and also proves that the tensegrity beam is sufficiently good for lightweight large-span structural applications.

Figure 7 plots the internal forces over time of typical cable elements excited by two different seismic waves, correspondingly, the results of the internal forces over time of typical struts elements are plotted in Figure 8. Obviously, the results from Figures 7–8 show that the changes of internal force in typical cable elements and strut elements are within 350 N and 800 N, respectively. In other words, the maximum variation amplitudes of cables and struts are with 8% and 9%, respectively. This indicates that all these typical cable elements and strut elements remain in tension and compression at all times, respectively.
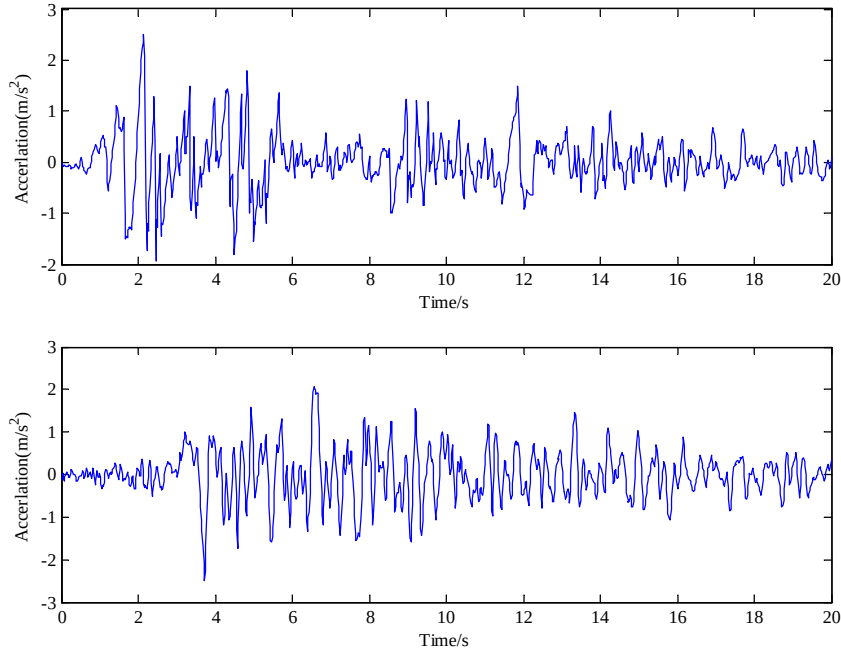
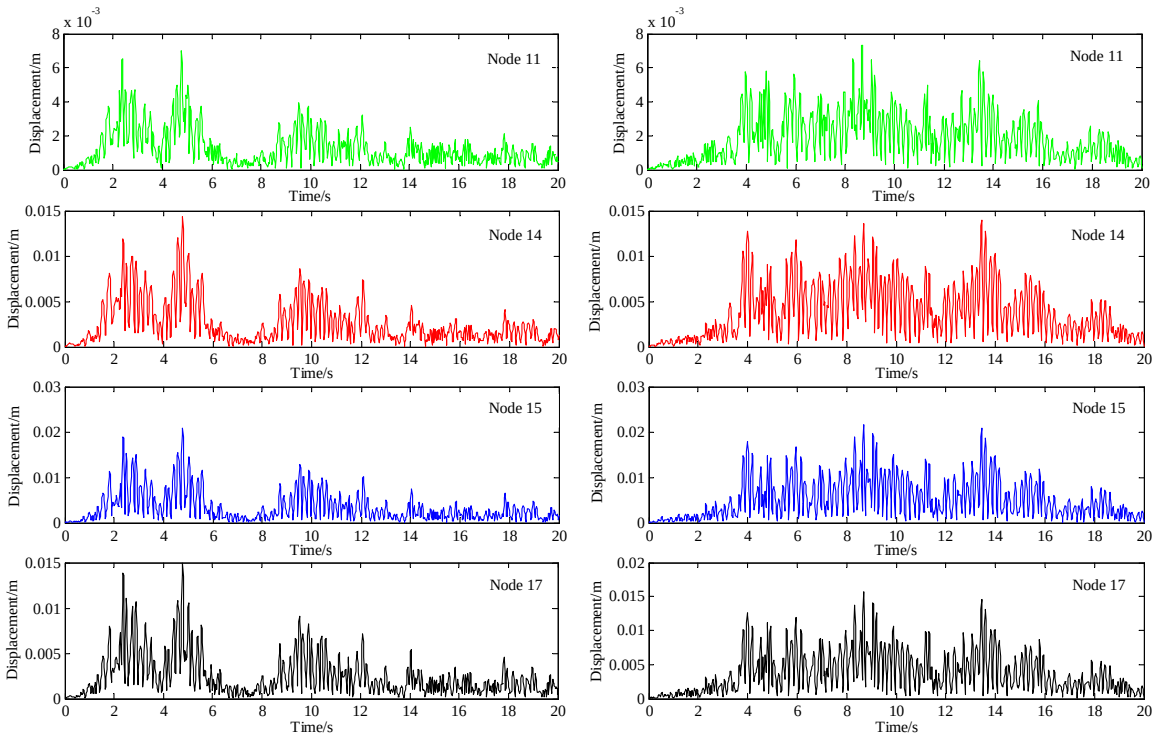**Figure 5.** Seismic wave with peak value of 250 Gal. Top: El Centro; bottom: Taft.

Figure 6. Displacements over time of typical nodes excited by different seismic waves.
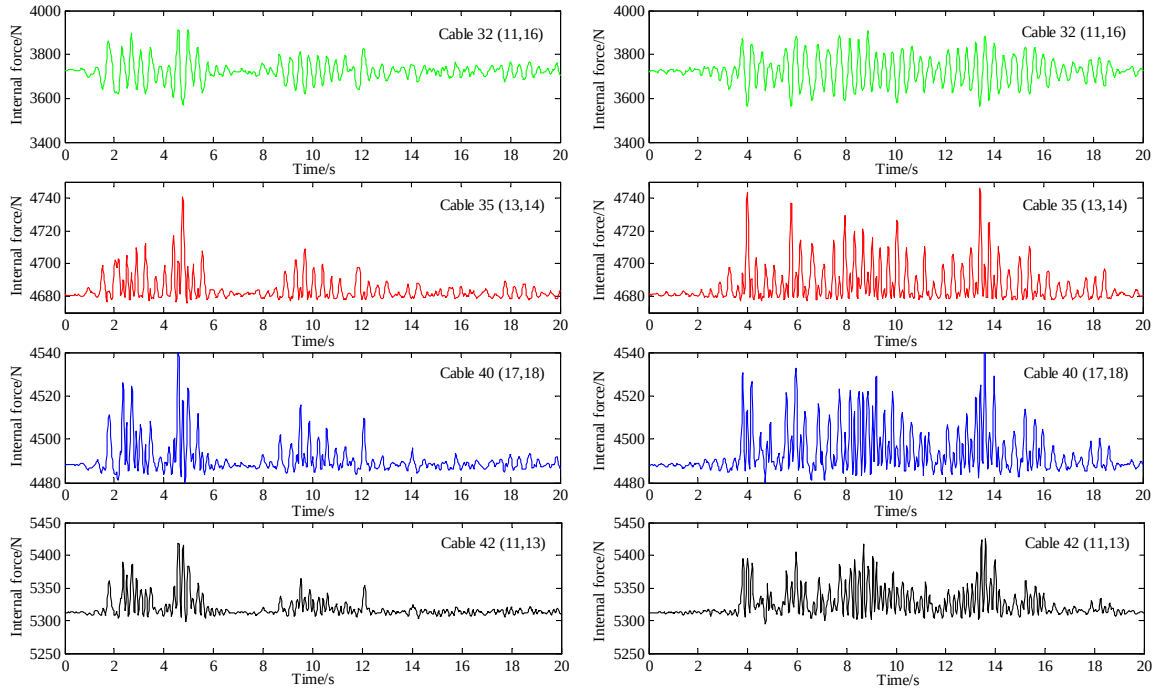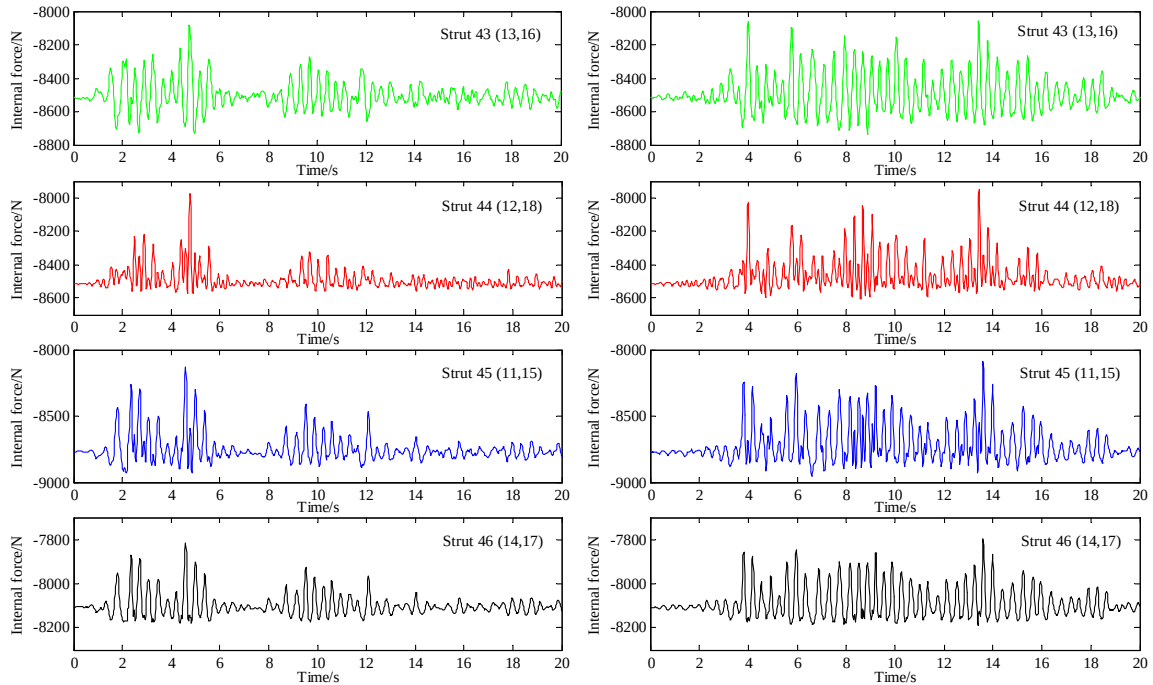Left column: El Centro; right column: Taft.

Figure 7. Internal forces over time of typical cable elements excited by different seismic waves. Left column: El Centro; right column: Taft.

That is to say, none of the components of this tensegrity beam with the properties given in Table 1 will be laid off due to the tension in struts or slackening of cables. The whole system works in the elastic range, and the structure has good seismic performance.

Table 3 gives the comparison of the maximum stresses of the specified elements excited by two seismic waves. As can be seen, the maximum elemental stresses (including cables and struts) are very close to each other for the two different seismic waves, demonstrating the phenomenon that the stress distributions of cables or struts are almost the same for the structure excited by these two seismic waves.

Finally, Table 4 gives the comparison of the convergence and efficiency of three different methods, and highlights that the CR formulation presented here is much faster than previous nonlinear formulations based on the total Lagrangian or updated Lagrangian solutions.

Node	11	14	15	17
El Centro	0.0070 m	0.0143 m	0.0209 m	0.0149 m
Taft	0.0073 m	0.0139 m	0.0217 m	0.0157 m

Table 3. Comparison of the maximum displacements of the specified nodes under two different seismic waves.

Figure 8. Internal forces over time of typical strut elements excited by different seismic waves. Left column: El Centro; right column: Taft.

	Taft seismic wave			El Centro seismic wave		
Comparison	TL	UL	CR	TL	UL	CR
Convergence	yes	yes	yes	yes	yes	yes
Total number of iterations	2352	1986	534	2332	1896	521
CPU times	55.29	42.38	19.68	54.89	42.02	19.23

Table 4. Efficiency comparison of formulations for a five-quadruplex module tensegrity beam.

5. Conclusion

We have presented a new three-dimension corotational algorithm to investigate the nonlinear dynamic properties of tensegrity structures. A new dynamic tangent stiffness matrix of a space rod element is derived based on the corotational approach which decomposes a large displacement into a large rigid body motion and a small strain, thus the behavior of elements can be described directly in the local coordinate system utilizing an engineering strain. It is very convenient for implementation of a standard finite element procedure. The validity and efficiency of the proposed method are illustrated by numerical examples. Dynamic responses of tensegrities, including a classical tensegrity quadruplex unit and a five-module quadruplex module tensegrity beam are investigated using the proposed formulation. The outcomes of the proposed study also confirm that the CR approach is more efficient and practical than the

TL and UL formulations of the elements in the structure that have more rigid body modes of translation and rotation than they have deformation modes.

It should be noted that, however, the proposed formulation is not valid for large-strain deformation. Nevertheless, combining with other approaches or technics [Shekastehband et al. 2012; Shekastehband and Abedi 2013], the proposed method could be extended to predict collapse of a tensegrity due to fracture of cables or buckling of bars, i.e. once the axial stress-axial strain behaviors of struts and cables are evaluated by the proposed method, a nonlinear dynamic collapse analysis can then be performed to find the load-deflection responses of the tensegrity system. Additionally, dynamic elasto-plastic behavior and vibration control of tensegrity structures, especially active tensegrities, e.g., deployable tensegrities and clustered tensegrities, need to be further investigated. These are some directions for future work.

Acknowledgements

References

[Adam and Smith 2008] B. Adam and I. F. C. Smith, "Active tensegrity: a control framework for an adaptive civil-engineering structure", *Comput. Struct.* **86** (2008), 2215–2223.

[Barnes 1999] M. R. Barnes, "Form finding and analysis of tension structures by dynamic relaxation", *Int. J. Space Struct.* **14** (1999), 89–104.

[Chen et al. 2012] Y. Chen, J. Feng, and Y. Wu, "Novel form-finding of tensegrity structures using ant colony systems", *J. Mech. Robot.* **4** (2012), 031001.

[Crisfield and Moita 1996] M. A. Crisfield and G. F. Moita, "A unified co-rotational framework for solids, shells and beams", *Int. J. Solids Struct.* **33** (1996), 2969–2992.

[Domer and Smith 2005] B. Domer and I. F. C. Smith, "An active structure that learns", *J. Comput. Civil. Eng.* **19** (2005), 16–24.

[Eriksson and Faroughi 2013] A. Eriksson and S. Faroughi, "Quasi-static inflation simulations based on co-rotational triangular space membrane elements", *Int. J. Struct. Stab. Dyn.* **13** (2013), 714–733.

[Faroughi and Eriksson 2017] S. Faroughi and A. Eriksson, "Co-rotational formulation for dynamic analysis of space membranes based on triangular elements", *Int. J. Mech. Mater. Des.* **13** (2017), 229–241.

[Faroughi and Lee 2014] S. Faroughi and J. Lee, "Geometrical nonlinear analysis of tensegrity based on a co-rotational method", *Adv. Struct. Eng.* **17** (2014), 41–52.

[Faroughi et al. 2015] S. Faroughi, H. H. Khodaparast, and M. I. Friswell, "Non-linear dynamic analysis of tensegrity structures using a co-rotational method", *Int. J. Non-Linear Mech.* **69** (2015), 55–65.

[Faroughi et al. 2017] S. Faroughi, H. H. Khodaparast, M. I. Friswell, and S. H. Hosseini, "A shape memory alloy rod element based on the co-rotational formulation for nonlinear static analysis of tensegrity structures", *J. Intell. Mater. Syst. Struct.* **28** (2017), 35–46.

[Felippa and Haugen 2005] C. A. Felippa and B. Haugen, "A unified formulation of small-strain corotational finite elements: I. Theory", *Comput. Methods Appl. Mech. Eng.* **194**:21-24 (2005), 2285–2335.

[Feng 2017] X. Feng, "The optimal initial self-stress design for tensegrity grid structures", *Comput. Struct.* **193** (2017), 21–30.

[Feng and Guo 2015] X. Feng and S. Guo, "A novel method of determining the sole configuration of tensegrity structures", *Mech. Res. Commun.* **69** (2015), 66–78.

[Feng and Guo 2017] X. Feng and S. Guo, "Geometrical nonlinear elasto-plastic analysis of tensegrity systems via the co-rotational method", *Mech. Res. Commun.* **79** (2017), 1–11.

[Guest 2006] S. Guest, "The stiffness of prestressed frameworks: a unifying approach", *Int. J. Solids Struct.* **43** (2006), 842–854.

[Juan and Tur 2008] S. H. Juan and J. M. M. Tur, "Tensegrity frameworks: Static analysis review", *Mech. Mach. Theory* **43**:7 (2008), 859–881.

[Kahla and Kebiche 2000] N. B. Kahla and K. Kebiche, "Nonlinear elastoplastic analysis of tensegrity systems", *Eng. Struct.* **22** (2000), 1552–1566.

[Kebiche and Kahla 2000] K. Kebiche and N. B. Kahla, "Nonlinear elastoplastic analysis of tensegrity systems", *Eng. Struct.* **23** (2000), 1552–1566.

[Kebiche et al. 1999] K. Kebiche, M. N. Kazi-Aoual, and R. Motro, "Geometrical non-linear analysis of tensegrity systems", *Eng. Struct.* **21** (1999), 864–876.

[Kim and Yong 2001] J. H. Kim and H. K. Yong, "A predictor-corrector method for structural nonlinear analysis", *Comput. Methods Appl. Mech. Eng.* **191** (2001), 959–974.

[Koohestani and Guest 2013] K. Koohestani and S. D. Guest, "A new approach to the analytical and numerical form-finding of tensegrity structures", *Int. J. Solids Struct.* **50** (2013), 2995–3007.

[Korkmaz 2011] S. Korkmaz, "A review of active structural control: challenges for engineering informatics", *Comput. Struct.* **89** (2011), 2113–2132.

[Le et al. 2011] T. N. Le, J. M. Battini, and M. Hjiaj, "Efficient formulation for dynamics of corotational 2D beams", *Comput. Mech.* **48** (2011), 153–161.

[Le et al. 2012] T. N. Le, J. M. Battini, and M. Hjiaj, "Dynamics of 3D beam elements in a corotational context: a comparative study of established and new formulations", *Finite Elem. Anal. Des.* **61** (2012), 97–111.

[Lee and Lee 2014] S. Lee and J. Lee, "Form-finding of tensegrity structures with arbitrary strut and cable members", *Int. J. Mech. Sci.* **85** (2014), 55–62.

[Luo et al. 2008] Y. Luo, X. Xu, T. Lele, S. Kumar, and D. E. Ingber, "A multi-modular tensegrity model of an actin stress fiber", *J. Biomech.* **41** (2008), 2379–2387.

[Masic and Skelton 2006] M. Masic and R. E. Skelton, "Selection of prestress for optimal dynamic/control performance of tensegrity structures", *Int. J. Solids Struct.* **43** (2006), 2110–2125.

[Murakami 2001] H. Murakami, "Static and dynamic analyses of tensegrity structures. Part 1. Nonlinear equation of motion", *Int. J. Solids Struct.* **38** (2001), 3599–3613.

[Oliveto and Sivaselvan 2011] N. D. Oliveto and M. V. Sivaselvan, "Dynamic analysis of tensegrity structures using a complementarity framework", *Comput. Struct.* **89** (2011), 2471–2483.

[Paul et al. 2006] C. Paul, F. Valero-Cuevas, and H. Lipson, "Design and control of tensegrity robots for locomotion", *IEEE Trans. Robot.* **22** (2006), 944–957.

[Raja and Narayanan 2007] M. G. Raja and S. Narayanan, "Active control of tensegrity structures under random excitation", *Smart Mater. Struct.* **16** (2007), 809–817.

[Rovira and Tur 2009] A. G. Rovira and J. M. M. Tur, "Control and simulation of a tensegrity-based mobile robot", *Robot. Auton. Syst.* **57** (2009), 526–535.

[Shekastehband and Abedi 2013] B. Shekastehband and K. Abedi, "Collapse behavior of tensegrity systems due to cable rupture", *Int. J. Struct. Stab. Dyn.* **13** (2013), 1250079.

[Shekastehband et al. 2012] B. Shekastehband, K. Abedi, N. Dianat, and M. R. Chenaghlou, "Experimental and numerical studies on the collapse behavior of tensegrity systems considering cable rupture and strut collapse with snap-through", *Int. J. Non-Linear Mech.* **47** (2012), 751–768.

[Skelton et al. 2014] R. E. Skelton, F. Fraternali, G. Carpentieri, and A. Micheletti, "Minimum mass design of tensegrity bridges with parametric architecture and multiscale complexity", *Mech. Res. Commun.* **58** (2014), 124–132.

[Sultan and Skelton 2003] C. Sultan and R. Skelton, "Deployment of tensegrity structures", *Int. J. Solids Struct.* **40** (2003), 4637–4657.

[Tibert and Pellegrino 2003] A. G. Tibert and S. Pellegrino, "Review of form-finding methods for tensegrity structures", *Int. J. Space Struct.* **18** (2003), 209–223.

[Tran and Lee 2010] H. C. Tran and J. Lee, "Self-stress design of tensegrity grid structures with exostresses", *Int. J. Solids Struct.* **47** (2010), 2660–2671.

[Tran and Lee 2011] H. C. Tran and J. Lee, "Geometric and material nonlinear analysis of tensegrity structures", *Acta Mech. Sinica* **27**:6 (2011), 938–949.

[Wroldsen et al. 2009] A. S. Wroldsen, M. C. de Oliveira, and R. E. Skelton, "Modelling and control of non-minimal non-linear realisations of tensegrity systems", *Int. J. Control* **82** (2009), 389–407.

[Xu and Luo 2010] X. Xu and Y. Luo, "Form-finding of nonregular tensegrities using a genetic algorithm", *Mech. Res. Commun.* **37** (2010), 85–91.

[Zhang et al. 2013] L. Zhang, Q. Gao, and H. W. Zhang, "An efficient algorithm for mechanical analysis of bimodular truss and tensegrity structures", *Int. J. Mech. Sci.* **70** (2013), 57–68.

[Zhang et al. 2014] L.-Y. Zhang, Y. Li, Y.-P. Cao, and X.-Q. Feng, "Stiffness matrix based form-finding method of tensegrity structures", *Eng. Struct.* **58** (2014), 36–48.

[Zhang et al. 2015] L. Zhang, M. K. Lu, H. W. Zhang, and B. Yan, "Geometrically nonlinear elasto-plastic analysis of clustered tensegrity based on the co-rotational approach", *Int. J. Mech. Sci.* **93** (2015), 154–165.

[Ziegler 2005] F. Ziegler, "Computational aspects of structural shape control", *Comput. Struct.* **83** (2005), 1191–1204.

XIAODONG FENG: `xiaodong.feng@csu.edu.cn`
School of Civil Engineering, Shaoxing University, Shaoxing, 312000, China

msp

JOURNAL OF MECHANICS OF MATERIALS AND STRUCTURES

msp.org/jomms

Founded by Charles R. Steele and Marie-Louise Steele

See msp.org/jomms for submission guidelines.

Journal of Mechanics of Materials and Structures

Volume 13, No. 3   May 2018